Peer reviewed version of the manuscript published in final form at ACS Synthetic Biology (2021) DOI:10.1021/acssynbio.1c00336.

Kinetics of RNA and RNA:DNA hybrid strand displacement

Hao Liu,[†] Fan Hong,[‡] Francesca Smith,[¶] John Goertz,[¶] Thomas Ouldridge,[§] Molly M. Stevens,[¶] Hao Yan,[†] and Petr Šulc[*,†]

[†]*Center for Molecular Design and Biomimetics at the Biodesign Institute and School of Molecular Sciences, Arizona State University, Tempe, Arizona 85287, USA*

[‡]*Wyss Institute for Biologically Inspired Engineering, Harvard University, Boston, MA 02115, USA*

[¶]*Department of Materials, Department of Bioengineering and Institute of Biomedical Engineering, Imperial College London, London, SW7 2AZ, UK*

[§]*Department of Bioengineering, Imperial College London, London, SW7 2AZ, UK*

E-mail: psulc@asu.edu

Abstract

In nucleic acid nanotechnology, strand displacement is a widely used mechanism where one strand from a hybridized duplex is exchanged with an invading strand that binds to a toehold, a single-stranded region on the duplex. It is used to perform logic operations on a molecular level, initiate cascaded reactions, or even for in vivo diagnostics and treatments. While systematic experimental studies have been carried out to probe the kinetics of strand displacement in DNA with different toehold lengths, sequences and mismatch positions, there has not been a comparable investigation of RNA or RNA-DNA hybrid systems. Here, we experimentally study how toehold length, toehold location (5′ or 3′ end of the strand) and mismatches influence the strand displacement kinetics. We observe reaction acceleration with increasing toehold length

and placement of toehold at 5′ end of the substrate. We find that mismatches closer to the interface of toehold and duplex slow down the reaction more than remote mismatches. Comparison of RNA and DNA displacement with hybrid displacement (RNA invading DNA or DNA invading RNA) is partly explainable by the thermodynamic stabilities of the respective toehold regions, but also suggest that the rearrangement from B-form to A-form helix in case of RNA invading DNA might play a role in the kinetics.

Keywords

RNA nanotechnology, DNA nanotechnology, Strand displacement, DNA:RNA hybrid duplex, Kinetics

Introduction

DNA and RNA play essential roles in all living systems. Besides their importance in biology, nucleic acids have also become essential in nanotechnology applications due to their structural diversity and the programmability, enabled by base pairing between complementary strands. In the past few decades, the fields of DNA and RNA nanotechnology have led to the design of increasingly complex nanostructures and devices self-assembled from DNA and/or RNA, with applications ranging from photonics and nanofabrication to drug delivery, medical treatment and diagnostics.[1–4]

A key mechanism in the field of nucleic acid nanotechnology is the strand displacement reaction.[5,6] Starting from the pioneering work of DNA nanotweezers done by Yurke et al,[7] toehold mediated strand displacement (TMSD) has been employed to construct dynamic nucleic acid systems. The process has found a wide range of applications that include diagnostics,[3] reconfigurable and dynamic nanostructures,[8,9] nanomotors[10] and molecular computation.[11–13] It is also likely involved in interactions between RNA molecules in biological systems.[14] Recent experimental studies have shown that internal strand displacement (where

one part of RNA strand displaces other regions of the same RNA strand) is likely relevant to the SRP RNA kinetic folding pathway.[15]

The strand displacement reaction involves an invading strand (invader) that binds to a single-stranded region (toehold) on a complementary strand (substrate), displacing a partially complementary strand (incumbent); the initial substrate-incumbent complex is often referred to as a "gate". Readout is typically accomplished via an additional duplex (reporter) with fluorophore-modified ends; this reporter complex undergoes a second strand displacement reaction with the released incumbent, as illustrated in Fig. 1. In short, the strand displacement reaction describes the process in which the invader binds to the complementary, single-stranded region of substrate strand then processively displaces the substrate-bound incumbent strand base-by-base via a random walk until the latter is released. This hybridization reaction exchanges the incumbent strand from the duplex with the new invader and can therefore be used to initiate the conformational change or cascaded reactions. Furthermore, it has been shown that the combination of these reactions can realize complex logic functions, where the input is presence or absence of a particular strand.[13] The presence of a toehold increases the probability of successful displacement after binding and hence speeds up the kinetics of the removal of the incumbent strand by the invader, with the speed increasing with longer toeholds.[6]

In addition to the extensive usage of DNA strand displacement in nanodevices, RNA and RNA:DNA hybrid stand displacement are also of great interest due to their potential in *in vivo* applications, ranging from synthetic biology to diagnostics.[16] Moreover, the RNA:DNA hybrid strand displacement is also speculated to be be involved in the gene editing process of CRISPR-Cas9 system, where the formation of R-loop requires the base flipping in the target DNA double strand for crRNA to bind with the assistance of nearby amino acids.[17,18] The transition of a DNA-DNA duplex to RNA-DNA hybrid duplex could be rationalized with a strand displacement process.[19,20] Further experimental efforts are necessary to verify the hypothesis while more insights could also be gained through studying the RNA:DNA hybrid

strand displacement system in isolation.

The efforts to understand the mechanism of strand displacement likely began with the initial studies of branch migration.[21,22] Yurke and Mills[23] first identified the phenomena of exponential acceleration of the rate constant with the increasing toehold length with the study of kinetics. Zhang and Winfree[6] then studied the mechanism of DNA strand displacement through a systematic kinetics experiment that revealed reaction acceleration saturated at a toehold length of around 6 nucleotides (nt). The authors proposed a quantitative model of DNA strand displacement with varying toehold length. Srinivas et al[24] then proposed the "Intuitive Energy Landscape" (IEL) model that sought to predict strand displacement rates from basepair level thermodynamics. This model has been further extended by Irmisch *et al.*[25] A coarse-grained model of DNA[26] was also used to study strand displacement reactions through simulation, providing more structural and physical understanding of the underlying mechanism.[24] Furthermore, investigations into the effects of mismatched base pairs between the invader and the substrate in DNA TMSD have demonstrated that the kinetics are highly dependent on the position of the mismatch.[27–29]

A systematic study of RNA TMSD was performed *in silico* with oxRNA,[30] a coarse-grained model of RNA. Qualitatively similar dynamic behavior was observed compared to DNA strand displacement when the toehold length was varied,[31] with exponential speed-up of TMSD rate with increasing toehold length until the speed is saturated. Additionally, toehold location ($5'$ or $3'$) was also predicted to affect the reaction rate due to an extra cross-stacking interaction between the invader and substrate strands when toehold is located at the $5'$ end, which thus speeds up the reaction.

Recently, an experimental study has been carried out where an RNA strand invades a DNA duplex.[32] The authors compared DNA and RNA single strand invading DNA duplex with a long toehold, and found that the location of the toehold as well as the toehold sequence affected the kinetics of the displacement.

Here we study RNA-based strand displacement, considering pure RNA-based systems

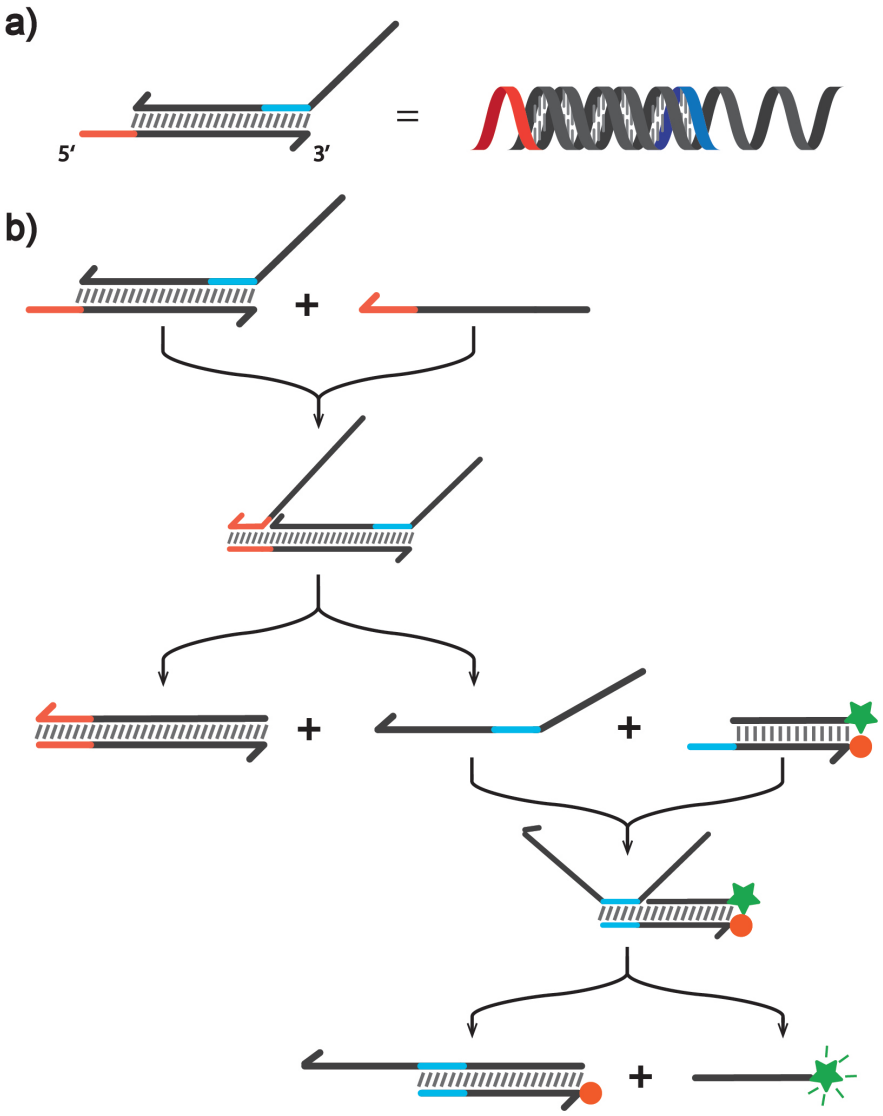

Figure 1: Schematic illustration of the experimental design of RNA strand displacement. a) Oligonucleotide strands are represented with a half headed arrow at the 3' end. Primary and reporter toeholds are colored orange and blue, respectively. b) To observe reaction progression, we used a reporter complex consisting of a FAM-labelled DNA strand hybridized to a TAMRA-labelled DNA strand, mixed in solution with the primary reaction system. Displacement of the (RNA) incumbent strand from the primary complex triggers the secondary strand displacement of FAM-labelled fluorescent strand via interaction with the reporter toehold on the TAMRA-labelled strand. This displacement leads to un-quenching of the FAM fluorescence, allowing us to monitor reaction progress through the FAM signal. Throughout this work, RNA duplexes are represented with *slanted* gray lines between the two strands, DNA duplexes are represented with *vertical* gray lines, and RNA-DNA hybrids are indicated by alternating slanted and vertical gray lines (not shown in thiss figure).

as well as hybrid systems with DNA invading an RNA duplex and RNA invading a DNA duplex. For the first time in experiment, we compare in one experimental set-up the effects of toehold length, toehold location, and mismatch location on strand displacement kinetics. Specifically, we examine how mismatches between the RNA invader and the substrate, as well as toehold positioned at either the $5'$ or $3'$ end of a substrate and finally toehold length when it is placed at the $5'$ end alter the reactions rate. The quantitative analysis of the kinetics result along with the qualitative modelling will be beneficial for further designs of RNA-involved strand displacement systems, especially in the fields of synthetic biology and RNA nanotechnology.

Results and Discussion

We designed a set of experiments to measure TMSD reaction kinetics. As schematically outlined in Fig. 1, the displaced incumbent strand then binds to a DNA reporter complex that produces a fluorescent signal to report on the reactions. To study the kinetics of RNA strand displacement, we consider systems of variable toehold lengths (from 1 to 6 nt) placed either at $3'$ or $5'$ end of the substrate. We additionally test systems where the invading RNA strand has a single mismatch with the substrate strand. We consider six different positions of the mismatch location. We further study the cases of hybrid RNA:DNA strand displacement, where either the DNA invader displaces incumbent RNA strand bound to an RNA substrate, or an RNA invader displaces DNA incumbent from a DNA substrate. The systems studied in experiment are schematically shown in Fig. 2.

The details of the experimental setup and the data fitting procedure are described in the Supplementary Material. The experimental results for the respective systems studied are provided below and the fitted rates of TMSD reactions for all the systems studied are shown in Table 1.

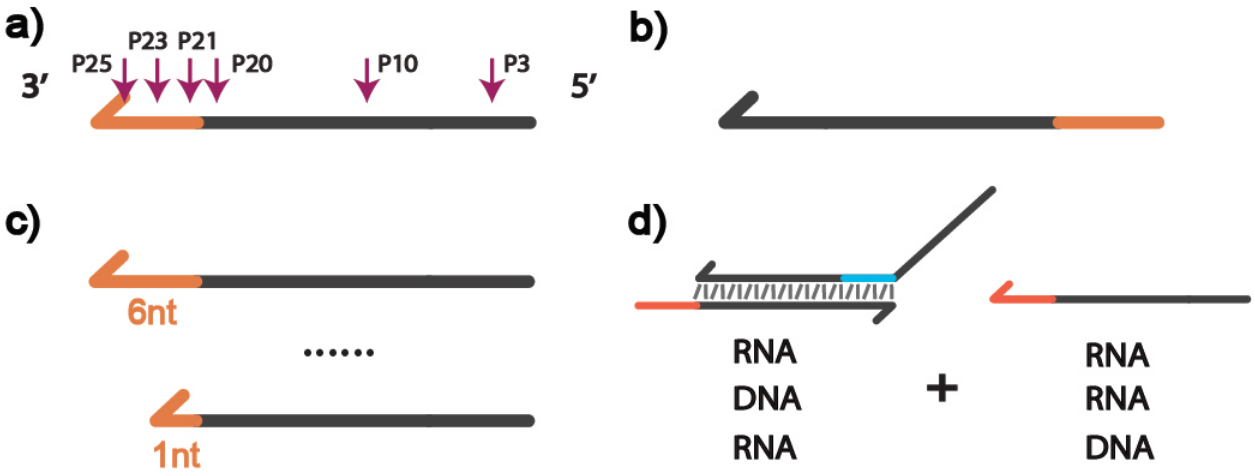

Figure 2: The design of the invader strand in different experiments. a) Mismatches are located at position 3 (U → C), 10 (C → A), 20 (C → A), 21 (C → A), 23 (G → A), or 25 (U → A) from the 5' end of the substrate strand (shown here on the invader strand). Positions 3, 10, and 20 are located in the branch migration region and the last three placed within the toehold. We only consider experiments where a single mismatch is present. b) We designed toeholds located either at the 5' end of the substrate strand and the 3' end of the invader (shown in (a) and in Fig. 1), referred to as simply a *3' toehold*, as well as toeholds located at the 3' end of the substrate strand and correspondingly at the 5' end of the invader (not shown here), referred to as a *5' toehold* . c) Toehold length was varied from 1 nucleotide (nt) to 6 nt on the invader. d) We investigated the scenarios of an RNA strand invading an RNA duplex (referred to as RNA:RNA), an RNA strand invading an DNA duplex (RNA:DNA), a DNA strand invading an RNA duplex (DNA:RNA), and a DNA strand invading a DNA duplex (DNA:DNA). In all cases the respective sequences are identical (with U substituting for T in case we compare RNA and DNA sequences).

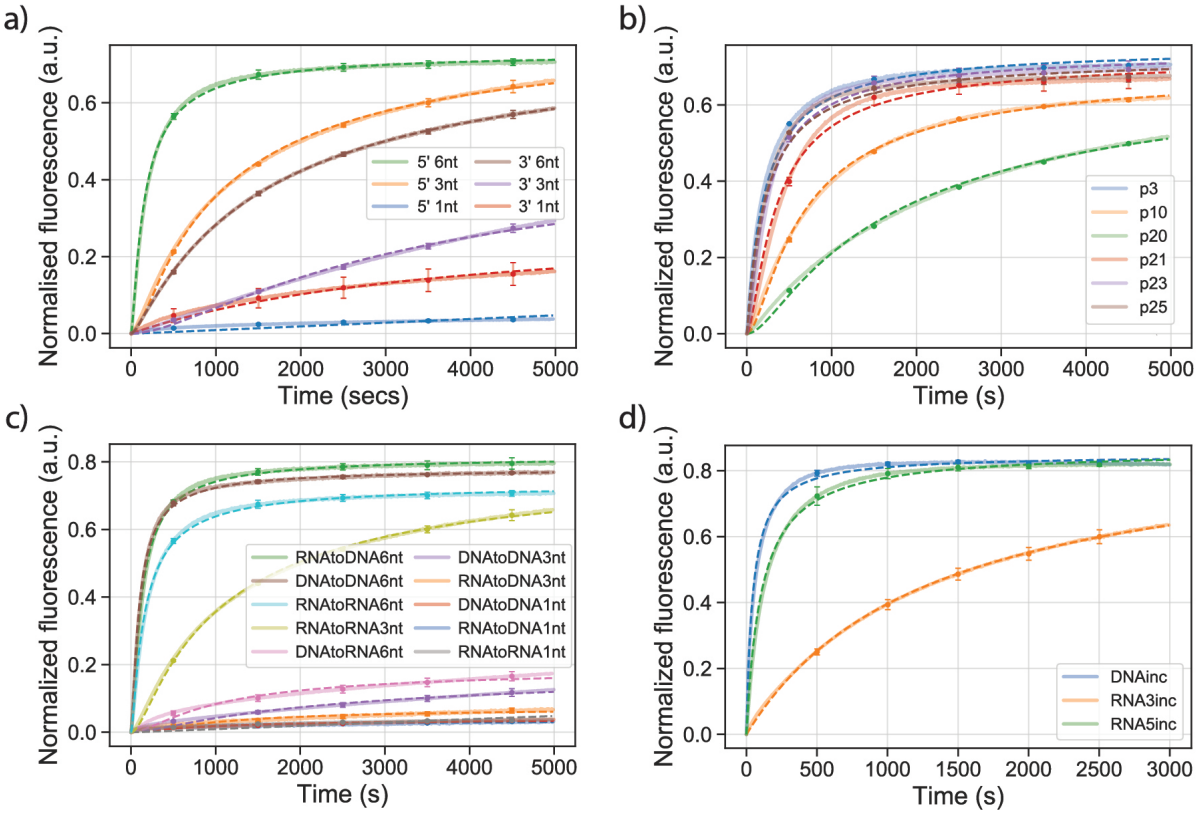

Figure 3: Summary of the kinetic profiles of RNA strand displacement experiments. Fluorescent signals are normalized according to the protocol described in data processing section. All curves, unless specified, correspond to reactions with 6 nt 5' toeholds. Solid, translucent lines indicate averaged experimental fluorescent trajectories while dotted lines represent the model fit. Error bars shown at 500s, 1500s, 2500s, 3500s and 4500s represent the standard deviation calculated from 3 replicate measurements; in some cases they are smaller than the symbol itself and not visible. a) RNA:RNA displacement with a 1, 3, or 6 nt toehold located at either 5' or 3' end. b) RNA:RNA displacement with a 5' toehold and mismatches placed in positions selected from either the branch migration domain or toehold domain. For example, p3 indicates a mismatch in the third base pair from the 5' end. c) RNA:RNA, DNA:DNA and RNA:DNA hybrid strand displacement curves with 1, 3 and 6 nt 5' toehold. d) Characterization of the reporter reaction between the incumbent strand and quenched (DNA) reporter complex to determine k_{rep}. Here, *RNA5inc* implies an RNA incumbent strand with the toehold placed at the 5' end.

Table 1: Rate constants obtained from fits to the experimental data in Fig. 3. k_{eff} is the effective rate constant for the displacements of the incumbent by invader. α is a scaling factor capturing the proportion of the maximum fluorescence signal achieved at equilibrium. Rate constants with low α value (< 0.70) are considered to align poorly with the assumptions of the fitted model and are labelled with an asterisk; they should not be treated as reliable. All the rate constants and the associated α are shown as the average of the fitting results of the three replicas and the calculated standard deviation is shown in the bracket. A 5 nt toehold sequence was investigated as well but was determined by native PAGE to exhibit excessive secondary structure, and so is omitted below.

Experiment		$\log_{10} k_{\text{eff}}$	α
RNA:RNA 5′ toehold	Toehold 1 nt	2.22 (0.05)	1.00 (0)
	Toehold 2 nt	4.44 (0.05)*	0.33 (0.02)
	Toehold 3 nt	4.37 (0.02)	0.77 (0.04)
	Toehold 4 nt	5.16 (0.17)	0.76 (0.03)
	Toehold 6 nt	6.25 (0.26)	0.73 (0.01)
	Mismatch P3	6.45 (0.23)	0.70 (0.02)
	Mismatch P10	4.64 (0.02)	0.71 (0.01)
	Mismatch P20	4.03 (0.01)	0.75 (0.01)
	Mismatch P21	5.16 (0.04)	0.72 (0.03)
	Mismatch P23	5.65 (0.08)	0.73 (0.02)
	Mismatch P25	5.99 (0.15)	0.71 (0.02)
RNA:RNA 3′ toehold	Toehold 1 nt	8.00 (0)*	0.30 (0.04)
	Toehold 3 nt	4.40 (0.09)*	0.68(0.03)
	Toehold 6 nt	5.90 (0.22)	0.77(0.01)
RNA:DNA 5′ toehold	Toehold 1 nt	4.03 (2.81)*	0.68 (0.45)
	Toehold 3 nt	6.05 (0.41)*	0.07 (0.01)
	Toehold 6 nt	5.72 (0.08)	0.81 (0.01)
DNA:DNA 5′ toehold	Toehold 1 nt	7.09 (0.77)*	0.04 (0.01)
	Toehold 3 nt	4.56 (0.12)*	0.1 (0.03)
	Toehold 6 nt	5.97 (0.14)	0.77 (0.01)
DNA:RNA 5′ toehold	Toehold 6 nt	5.33 (0.03)*	0.19 (0.01)

Effects of toehold length and location

We first studied the effects of toehold length on RNA:RNA TMSD kinetics with the toehold placed at the 5′ end of the substrate. We considered toehold lengths 1, 2, 3, 4 and 6 nucleotides, as the reaction with 5nt-toehold involved a gate with unexpected secondary structures (Figure S4). As shown in the Fig. 3a and Table 1, a clear trend emerges that increasing the toehold length accelerates the reaction rate for the 5' end toehold location. This trend is also observed for the 3' end toehold location. We observe that for toeholds longer than 2 nucleotides, the fitted reaction rate increases by about a factor of 6 to 10 for each additional nucleotide in the toehold domain (Table 1).

This behavior is in agreement with previous experimental measurements for DNA[6,24] as well as simulation studies of RNA TMSD.[31] For shorter toeholds, the probability of the invader binding to the substrate decreases as the weaker interaction strength leads to frequent binding and unbinding of the invader from the toehold. Once the free energy of binding to the toehold becomes sufficiently strong, the rate of displacement saturates, as the probability of unbinding is so small that the invader always completes the strand displacement after binding to the toehold.

We note that we had difficulties fitting the reaction rates to fluorescent signal for toehold lengths 1 and 2, presumably due to the weak signal that has not saturated even over the duration of the experimental measurements. The experimental measurements are shown in Fig. S5.

We next compared the dependence of TMSD kinetics on the placement of the toehold at either the 5′ or 3′ end of the substrate. This comparison has not previously been performed in a systematic study for RNA strand displacement. However coarse-grained simulations of TMSD for RNA predicted a speed-up of the reaction if the toehold is placed at the 5′ end of the substrate.[31] This phenomenon was attributed to the additional cross-stacking interaction between the invader and substrate strand at its 5' end due to the A-form helix structure of the RNA duplex. This structure should provide extra stabilization relative to when the the

invader binds to 3′ toehold. The simulations predict that strand displacement is faster by about a factor 2 to 10 for shorter toeholds until the rate of TMSD is saturated (which is at about 6 base pairs for average-strength sequences).[31]

We measured the rate of TMSD for toeholds of length 1, 3 and 6 nucleotides placed at 3′ end, which were designed so that the free energy of invader binding to them would be the same as the free energy of binding to toehold of the same length at 5′ end, exluding the putative cross-stacking contribution (see Supplementary Material). For the 3 nt toeholds, the fitted TMSD rate k_{eff} at the 3′ end was comparable to the 5′ end. For the toehold length 6 nt, the toehold placed at 5' end had approximately twenty times faster rate of TMSD than the one placed at the 3' end. We were unable to fit the rates for toeholds of length 1 nt, as the signal was very weak over the duration of the experiment. These results are in contrast with the simulations, where the rates of displacament were faster for the 5' end placement for 3nt length by about a factor of 2, and were comparable for 6 nt length. It is possible that there are additional sequence-dependent effects that can play role in the TMSD kinetics.

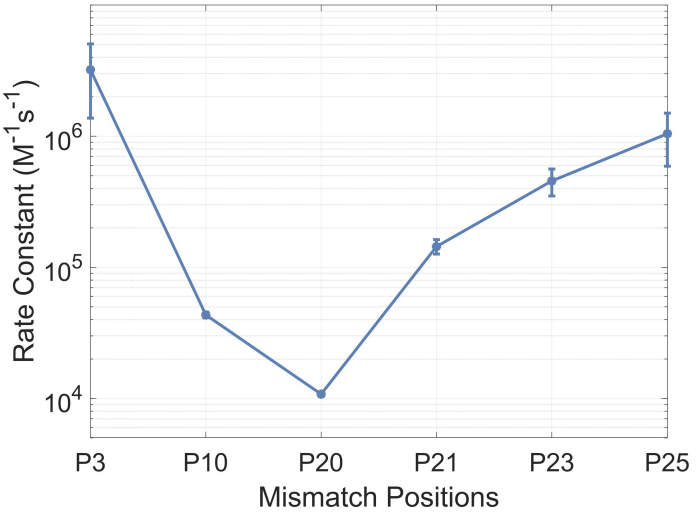

Figure 4: The fitted rate constants of reactions with different mismatches.

Mismatch effects

We further study the effects of mismatches between the invader RNA strand and the RNA substrate. For each system studied, we introduce a single mismatch in the RNA invader which could form neither Watson-Crick nor wobble complementary base pairing with the corresponding base on the substrate. For all the experiments with the mismatches, we consider substrate with toehold length 6 nt placed at the 5′ end. We only introduce a single mismatch in each experimentally studied system, and consider 6 different mismatch positions in the invader, as shown schematically in Fig. 2a. The mismatches are present either in the toehold binding region (P25, P23 or P21), in the first base pair next to the toehold end (P20), in the middle of invader (P10) and three bases from the end (P3). The experimental measurements are shown in Fig. 3 along with the fitted rates in Table 1 and in Fig. 4.

We observe that all considered mismatch positions lead to a slow-down of the reaction. However, the effects of the mismatch depend on the position with respect to the interface where the toehold region ends and the incumbent region begins: position P21 of the invader is the last base of the toehold region and P20 is the first base which displaces the incumbent. We observe that the largest slowdown (by about a factor of 134) is for the mismatch at P20 (Fig. 4), and the smallest effect for the mismatch at the end of furthest point away from the toehold (P3). For the mismatches in the toehold region (P25-P21), we find that the closer the mismatch is to the interface, the bigger the slowdown (by up to a factor of 7 difference between the furthest and closest points). Finally, for the mismatches in the incumbent displacement region, P20, P10 and P3, P20 has a much larger slowdown than P10, which in turn has a much larger slowdown than P3.

The observed slowdown induced by mismatches at different positions for RNA TMSD is compatible with the kinetics of TMSD of DNA strands with mismatches observed in computational and experimental studies.[25,27,28] The kinetics of the TMSD can be approximately modeled as a stochastic Markovian process consisting of transitions between states characterized by the number of bonds between respective strands.[24] This stochastic process can be

understood as a random walk on the free-energy profile of displacement, as illustrated in Figure S8. Introducing a mismatch between the invader and the substrate in the displacement region creates a free-energy barrier that increases the time it takes the invader to displace the substrate. The kinetics of the strand displacement is more affected by the mismatches closer to the toehold interface, as it increases the likelihood of the invader detaching from the toehold before successfully displacing the incumbent. Mismatches further from the interface have a smaller effect on the rate because systems that reach the mismatch location have a higher probability of nonetheless continuing to complete displacement if the mismatch is encountered later. The possibility of the substrate strand spontaneously detaching from a state with a small number of remaining base pairs enhances this effect.

RNA:DNA hybrid strand displacement

We next compare the hybrid TMSD systems where either DNA invades RNA duplex (DNA:RNA) or RNA invades a DNA duplex (RNA:DNA). For the studied toehold lengths (1, 3 and 6 nt), we also compare the hybrid TMSD systems with experiments where RNA invades RNA duplex (RNA:RNA) and where DNA invades DNA duplex (DNA:DNA). For the corresponding experiments at a given toehold length, we use the same nucleic acid sequences for invader, substrate and incumbent strands (substituting U for T in the case of RNA). For all the studied hybrid systems and DNA:DNA systems, the toehold is placed at the 5' end of the substrate. The fitted TMSD rates are shown in Table 1 with the corresponding curves shown in Fig. 3c. Sequences are listed in the Supplementary Material (Tables S1-S4).

For the longest toehold considered (6 nt), we observed RNA:RNA to be fastest, then DNA:DNA, and then RNA:DNA ($\log_{10} k_{\text{eff}}$ of 6.3, 6.0, and 5.7 respectively); DNA:RNA did not produce reliable k_{eff} but clearly displayed the slowest rate (Fig. 3c). For the shorter toehold length of 3 nt, the RNA:RNA appears to be the fastest by visual inspection of the fluorescent signal (Fig. 3), followed by DNA:DNA and then RNA:DNA. We did not study DNA:RNA for 3nt toehold. We note that RNA:DNA and DNA:DNA reactions were not

reliably fit with with our model (see Table 1), presumably since the reaction was too slow and did not reach equilibrium within the time of the experiment.

We rationalize the observed behavior of hybrid strand displacement through free-energy landscapes and known thermodynamic stabilities of duplexes of DNA, RNA, and RNA:DNA hybrids respectively.[33–35] The estimated free-energy profiles for the TMSD, based on intuitive energy landscape from Ref.,[24] as shown in Figure S8, including all the possible hybrid reaction scenarios with 6 or 3 nt toehold. Such free-energy landscapes have been used in prior studies for DNA.[36] For the same sequence, RNA:RNA toehold binding has the largest stability, followed by RNA:DNA and DNA:DNA respectively. Once the invader is bound to the toehold, it can either dissociate (overcoming the barrier given by binding to the toehold) or it can displace the incumbent. After overcoming the initial barrier to the displacement (about $2\,k_{\mathrm{B}}T$), the invader replaces the incumbent through branch migration process. For RNA:RNA or DNA:DNA TMSD systems, the newly created base pairs have identical stability, while for RNA:DNA, the new bases are on average more stable than the original ones, leading to a downhill free-energy landscape. For DNA:RNA, the newly created base pairs are less stable, so the branch migration part of TMSD corresponds to an uphill free-energy landscape. We note, however, that DNA:DNA reaction appears slightly faster than RNA:DNA for 6nt toehold system, despite the fact that the free-energy landscape is downhill for the RNA:DNA system due to the higher stability of the newly created base pairs. Since RNA:DNA hybrid duplex is known to prefer A-form helix, as opposed to the B-form typical for DNA duplexes, we hypothesize that the rearrangement from B-form helix into A-form might also affect the displacement rate.

The higher stability of the RNA:RNA toehold than the RNA:DNA toehold likely contributes to the slightly faster rate for RNA:RNA 6 nt toehold than for the RNA:DNA and DNA:DNA systems with the same toehold length. For the sequences used for toeholds of 3 nt, the stability of RNA:RNA and RNA:DNA toehold is comparable, and hence the RNA:DNA is expected to proceed faster due to the higher stability of newly formed RNA base pairs in

the branch migration region.

Conclusion

In a series of experiments, we found that RNA-based TMSD exhibits similar phenomena to those observed in DNA in terms of the toehold length effects and mismatches between the invader and the substrate. Through the systematic study of RNA and RNA:DNA hybrid strand displacement with a focus on the effects of toehold length, toehold location, and mismatch location, we discovered that: (i) increasing the toehold length has a significant boost on strand displacement reaction rate, resulting in exponential speed-up of the displacement reaction until saturation speed is reached, consistent with phenomena previously observed for DNA TMSD;[6] (ii) placement of the RNA toehold at 5' end of substrate can accelerate the reaction for a 6nt toehold; (iii) base mismatches on the invader generally slow down the reaction, and the closer they are to to the interface of toehold and branch migration range the bigger the effect; (iv) for toehold of length 6nt, RNA invading RNA duplex is faster than RNA invading DNA duplex. For toehold of length 3 nt, we found RNA invading DNA TMSD to be faster than RNA invading RNA. However, there are several open questions left for further studies. For example, what is the maximal rate of RNA-based strand displacement? How much does the relative stability of RNA:DNA duplexes to DNA:DNA favour invasion by RNA? These questions likely require a broader study involving a number of distinct sequences in order to access the generic biophysics underlying the system.

As the emerging field of RNA nanotechnology evolves and *in vivo* applications continue to expand, understanding the kinetics of RNA strand displacement is of increasing importance. Hybrid displacement systems that interface DNA with RNA are of interest for DNA nanotechnology interfacing with biological systems. Additionally, strand displacement reactions of RNA and hybrid systems can play a role in natural biological processes. Our results provide first systematic study of RNA and RNA:DNA hybrid displacement kinetics

and will help in understanding the phenomena and in building stochastic models of TMSD reactions for RNA and RNA:DNA hybrids. Our measurements can help with parametrization of strand displacement kinetics dynamics tools[37] as well as with optimization of logic gates based on strand displacement processes for synthetic biology applications, where DNA or RNA-based gates need to interface with naturally occurring RNAs.

Methods

Sequence Design

The sequences for the strand displacement characterization are designed using NUPACK[38] to minimize undesired secondary structures. For the experiments where we compare the 3′ and 5′ toeholds, we designed the toehold sequences to have the same free-energy of binding to the invader and the first and last bases of the branch migration are set to be Gs to minimize the change of toehold stacking energy. For example, the 5' toehold is 5'-GACCAG–, the corresponding 3' toehold is –GACCAG-3', and the stacking base for the 5' toehold and 3' toehold are both Gs. All the sequences of RNA and DNA strands that were used in the experiments are listed in Table S1 - S4 and the NUPACK prediction on each strand is shown in Figure S1 - S3.

Experiment Design

A schematic illustration is shown in Figure 2. To study the mismatch effects on strand displacement, six mismatch positions, distributed within both branch migration and toehold ranges, are selected and changed to another nucleotide that will not pair to the corresponding nucleotide on the other strand. For the study of both mismatches and toehold length effects, the toehold is located at the 5' end of the substrate. The toehold length is varied from 1 nt to 6 nt.

Additionally, experiments with 3' end toehold are conducted for toehold lengths 1, 3, and

6 nucleotides. For RNA-DNA hybrid systems, we perform experiments where a) an RNA invader displaces a DNA incumbent strand from a DNA substrate, and b) a DNA invader displaces an RNA incumbent strand from an RNA duplex. As a control, strand displacement experiments with the same toeholds were performed for a pure DNA system. Although our experiments study RNA strand displacement, the reporter complex is DNA-based since the stability against degradation provided by DNA will is preferred.

Substrate Preparation

Nucleic acid oligonucleotides used here were purchased from Integrated DNA Technologies (IDT), and purified through denaturing poly-acrylamide gel electrophoresis. Where applicable, fluorophores were attached by IDT as well. The measured absorbance at 260 nm using Thermo Scientific™ NanoDrop 2000 along with the calculated extinction coefficient were used to determine concentrations. All double-stranded complexes were prepared through annealing processes in a thermocycler (Eppendorf) with different programs in 1X TAE Mg^{2+} buffer (Tris base 40 mM, acetic acid 20 mM, $EDTA \cdot Na_2 \cdot 12H_2O$ 2 mM, $(CH_3COO)_2Mg \cdot 4H_2O$ 12.5 mM). The RNA samples were annealed at 65 °C for 5 minutes and then brought down to 20 °C with a constant rate of 1 °C/min while for DNA samples, after 5 minutes of annealing in 90 °C , they were programmed to be cooled down to 20 °C with the same rate.

Fluorimetry Experiments

The fluorescent kinetics over the strand displacement time was monitored with a Nanolog fluorometer (Horiba Jobin Yvon). All kinetic experiments were performed at 25 °C in 1X TAE Mg^{2+} buffer in a lid-covered Hellma Analytics cuvette. To minimize the non-specific cohesion of nucleic acids under low concentration to the tubes wall, the sample to be measured with final concentration (60 nM) was diluted in the cuvette from 2 μM stock solution. To initiate the reaction, free incumbent was added to the reporter solution for characterization of the reporter TMSD reaction and incumbent-substrate complex was added to the mixture

of reporter and invader for characterization of full reaction kinetics.

Before the initiation of reaction, samples were equilibrated for at least 300s to allow sample temperature and fluorescent signal to stabilize. The addition of strands was kept was performed by rapidly pipetting the solution and data points collected at the first 12s were discarded due to the influence of pipetting. Cuvettes were thoroughly cleaned subsequently by Milli-Q purified water and pure ethanol and allowed to be fully dried for next measurement.

The parameters settings of the fluorescence measurements were as follows: 495 nm excitation, 1 nm excitation slit, 520 nm emission, 10 nm emission slit. Specifically, a 1 nm excitation slit was chosen to reduce photobleaching of the dye molecules while a 10 nm emission slit guaranteed a proper signal level to be observed. The signal was collected from 0 to 5000 s with 0.5 s integration time and 3 s intervals. Kinetics measurements were repeated 3 times.

Data processing

The fluorescent signal was normalized with respect to the positive control (60nM fluorescently-labelled strand) and the initial fluorescent signal at time t = 0, resulting in a time-dependent fluorescent signal between 0 and 1.

$$\mathrm{F_{norm}} = \frac{\mathrm{F_t} - \mathrm{F_0}}{\mathrm{F_{max}} - \mathrm{F_0}}.$$

The above equation describes the normalization procedure, in which $\mathrm{F_{norm}}$ represents the normalized fluorescence; $\mathrm{F_t}$ the raw fluorescence data; $\mathrm{F_0}$ the initial fluorescence prior to mixing; and $\mathrm{F_{max}}$ the maximum achievable fluorescence, as indicated by the positive control. The positive control consisted of observing the fluorescence change of 60 nM reporter strand only for 5000 seconds. Note that subtraction of the first fluorescence measurement post-initiation may introduce a source of error for very fast reactions. However, we do not observe significant difference in the resultant rate constant through introducing such a normalization method and for consistency we use this approach throughout this work. Based on these

normalized fluorescent signals we observed that most of the experimental systems reached equilibrium with fluorescent signal smaller than the maximum fluorescence predicted by the positive control. Following the approach previously employed for DNA,[6] we introduced an additional parameter α, which represents a scaling factor capturing the proportion of the maximum fluorescence signal achieved at equilibrium. Thus, intuitively, α represents the proportion of the $c_0 = 60\,\mathrm{nM}$ initial reporter concentration that actually reacted.

Data fitting

While different versions of fitting of TMSD reaction are considered in this paper (see Supp. Mat.), a general case can be represented as below:

$$\text{Invader} + \text{Gate} \xrightarrow{k_{\text{eff}}} \text{Incumbent} + \text{WasteB}$$
$$\text{Incumbent} + \text{Reporter} \xrightarrow{k_{\text{rep}}} \text{Signal} + \text{WasteT}$$

The reaction kinetics is assumed to be of second order and a notation for the related reaction species is used as: Invader (V), Gate (G), Incumbent (I), Reporter (R) and Signal (S). k_{eff} and k_{rep} are therefore the rate constants for the displacements of the incumbent by invader and the signal by incumbent respectively. The differential relation between each reaction species can be modelled as follows:

$$\begin{aligned}
\tfrac{\mathrm{d[V]}}{\mathrm{dt}} &= -\mathrm{k_{eff}[V][G]} \\
\tfrac{\mathrm{d[G]}}{\mathrm{dt}} &= -\mathrm{k_{eff}[V][G]} \\
\tfrac{\mathrm{d[I]}}{\mathrm{dt}} &= \mathrm{k_{eff}[V][G] - k_{rep}[I][R]} \\
\tfrac{\mathrm{d[R]}}{\mathrm{dt}} &= -\mathrm{k_{rep}[I][R]} \\
\tfrac{\mathrm{d[S]}}{\mathrm{dt}} &= \mathrm{k_{rep}[I][R]}
\end{aligned}$$

with initial conditions $\mathrm{[I](0) = [S](0) = [R](0) = c_0\alpha}$ and others set to 0. The best-fit k_{rep} and α parameters for the reporter characterisation experiments are determined (see Supplementary Table S5 and Figure 3d) and subsequently with the known k_{rep} using the outlined ODEs we fit values for k_{eff} and α to match the measured fluorescent signal. We constrain the upper and lower bounds $\log k_{\text{rep}}$ and $\log k_{\text{eff}}$ to 1 to 7 and 1 to 8, respectively.

The fitting method employed here corresponds to the method adapted from Ref.[6] We tried the method from[28] (see Supplementary Table S6 and Fig. S7) for fitting as well. However, the method from Ref.[28] assumes that the reporter reaction is much faster than the original strand displacement reaction, which is not fully justified for our system, hence we report here the fits from sets of equations described above.

Author Contribution

HL, PŠ, and FH designed the research. HL carried out the experiments. FS, HL, TO, MS, JG, and PŠ carried out data analysis and fitting. HY, FH and PŠ supervised the experiments. All authors discussed the results and wrote the manuscript.

Conflict of Interest

The authors declare no competing financial interest.

Acknowledgement

The authors thank Shuoxing Jiang, Erik Poppleton, Michael Matthies, Xu Zhou and Lan Liu for helpful discussion. TO is supported by a Royal Society University Research Fellowship. JG acknowledges support from the National Institute Of General Medical Sciences of the National Institutes of Health under Award Number F32GM131594. FS is supported by the UK Engineering and Physical Sciences Research Council (EPSRC) grant EP/S022856/1 for the Centre for Doctoral Training in BioDesign Engineering. M.S. acknowledges support from the Royal Academy of Engineering under the Chairs in Emerging Technologies scheme (CIET20214) and the EPSRC grant "IRC Next Steps Plus: A Smartphone Powered mRNA Sequence Detector" [EP/R018707/1]. P.Š. acknowledges startup funding from Arizona State University.

Supporting Information Available

The Supporting Information includes all sequences used in this work, analysis of their secondary structure with NUPACK, gel electrophoresis of different strands used, detailed description of the data fitting, as well as an approximate model of the free-energy landscape of the strand displacement.

References

(1) Li, S.; Jiang, Q.; Liu, S.; Zhang, Y.; Tian, Y.; Song, C.; Wang, J.; Zou, Y.; Anderson, G. J.; Han, J.-Y., et al. A DNA nanorobot functions as a cancer therapeutic in response to a molecular trigger in vivo. *Nature biotechnology* **2018**, *36*, 258.

(2) Qi, X.; Liu, X.; Matiski, L.; Rodriguez Del Villar, R.; Yip, T.; Zhang, F.; Sokalingam, S.; Jiang, S.; Liu, L.; Yan, H., et al. RNA Origami Nanostructures for Potent and Safe Anticancer Immunotherapy. *ACS nano* **2020**, *14*, 4727–4740.

(3) Pardee, K.; Green, A. A.; Takahashi, M. K.; Braff, D.; Lambert, G.; Lee, J. W.; Ferrante, T.; Ma, D.; Donghia, N.; Fan, M., et al. Rapid, low-cost detection of Zika virus using programmable biomolecular components. *Cell* **2016**, *165*, 1255–1266.

(4) Guo, P. The emerging field of RNA nanotechnology. *Nature nanotechnology* **2010**, *5*, 833.

(5) Simmel, F. C.; Yurke, B.; Singh, H. R. Principles and applications of nucleic acid strand displacement reactions. *Chemical reviews* **2019**, *119*, 6326–6369.

(6) Zhang, D. Y.; Winfree, E. Control of DNA strand displacement kinetics using toehold exchange. *Journal of the American Chemical Society* **2009**, *131*, 17303–17314.

(7) Yurke, B.; Turberfield, A. J.; Mills Jr, A. P.; Simmel, F. C.; Neumann, J. L. A DNA-fuelled molecular machine made of DNA. *Nature* **2000**, *406*, 605.

(8) Wei, B.; Ong, L. L.; Chen, J.; Jaffe, A. S.; Yin, P. Complex reconfiguration of DNA nanostructures. *Angewandte Chemie* **2014**, *126*, 7605–7609.

(9) Grossi, G.; Jepsen, M. D. E.; Kjems, J.; Andersen, E. S. Control of enzyme reactions by a reconfigurable DNA nanovault. *Nature communications* **2017**, *8*, 992.

(10) Wickham, S. F.; Endo, M.; Katsuda, Y.; Hidaka, K.; Bath, J.; Sugiyama, H.; Turberfield, A. J. Direct observation of stepwise movement of a synthetic molecular transporter. *Nature nanotechnology* **2011**, *6*, 166–169.

(11) Qian, L.; Winfree, E.; Bruck, J. Neural network computation with DNA strand displacement cascades. *Nature* **2011**, *475*, 368–372.

(12) Wilhelm, D.; Bruck, J.; Qian, L. Probabilistic switching circuits in DNA. *Proceedings of the National Academy of Sciences* **2018**, *115*, 903–908.

(13) Qian, L.; Winfree, E. Scaling up digital circuit computation with DNA strand displacement cascades. *Science* **2011**, *332*, 1196–1201.

(14) Hong, F.; Šulc, P. An emergent understanding of strand displacement in RNA biology. *Journal of structural biology* **2019**, *207*, 241–249.

(15) Angela, M. Y.; Gasper, P. M.; Cheng, L.; Lai, L. B.; Kaur, S.; Gopalan, V.; Chen, A. A.; Lucks, J. B. Computationally reconstructing cotranscriptional RNA folding from experimental data reveals rearrangement of non-native folding intermediates. *Molecular Cell* **2021**,

(16) Green, A. A.; Silver, P. A.; Collins, J. J.; Yin, P. Toehold switches: de-novo-designed regulators of gene expression. *Cell* **2014**, *159*, 925–939.

(17) Klein, M.; Eslami-Mossallam, B.; Arroyo, D. G.; Depken, M. Hybridization kinetics explains CRISPR-Cas off-targeting rules. *Cell reports* **2018**, *22*, 1413–1423.

(18) Anders, C.; Niewoehner, O.; Duerst, A.; Jinek, M. Structural basis of PAM-dependent target DNA recognition by the Cas9 endonuclease. *Nature* **2014**, *513*, 569.

(19) Josephs, E. A.; Kocak, D. D.; Fitzgibbon, C. J.; McMenemy, J.; Gersbach, C. A.; Marszalek, P. E. Structure and specificity of the RNA-guided endonuclease Cas9 during DNA interrogation, target binding and cleavage. *Nucleic acids research* **2015**, *43*, 8924–8941.

(20) Strohkendl, I.; Saifuddin, F. A.; Rybarski, J. R.; Finkelstein, I. J.; Russell, R. Kinetic basis for DNA target specificity of CRISPR-Cas12a. *Molecular cell* **2018**, *71*, 816–824.

(21) Radding, C. M.; Beattie, K. L.; Holloman, W. K.; Wiegand, R. C. Uptake of homologous single-stranded fragments by superhelical DNA: IV. Branch migration. *Journal of Molecular Biology* **1977**, *116*, 825 – 839.

(22) Green, C.; Tibbetts, C. Reassociation rate limited displacement of DNA strands by branch migration. *Nucleic Acids Research* **1981**, *9*, 1905–1918.

(23) Yurke, B.; Mills, A. P. Using DNA to power nanostructures. *Genetic Programming and Evolvable Machines* **2003**, *4*, 111–122.

(24) Srinivas, N.; Ouldridge, T. E.; Šulc, P.; Schaeffer, J. M.; Yurke, B.; Louis, A. A.; Doye, J. P.; Winfree, E. On the biophysics and kinetics of toehold-mediated DNA strand displacement. *Nucleic acids research* **2013**, *41*, 10641–10658.

(25) Irmisch, P.; Ouldridge, T. E.; Seidel, R. Modelling DNA-strand displacement reactions in the presence of base-pair mismatches. *Journal of the American Chemical Society* **2020**,

(26) Ouldridge, T. E.; Louis, A. A.; Doye, J. P. Structural, mechanical, and thermodynamic properties of a coarse-grained DNA model. *The Journal of chemical physics* **2011**, *134*, 02B627.

(27) Haley, N. E.; Ouldridge, T. E.; Geraldini, A.; Louis, A. A.; Bath, J.; Turberfield, A. J. Rational design of hidden thermodynamic driving through DNA mismatch repair. *bioRxiv* **2018**, 426668.

(28) Machinek, R. R.; Ouldridge, T. E.; Haley, N. E.; Bath, J.; Turberfield, A. J. Programmable energy landscapes for kinetic control of DNA strand displacement. *Nature communications* **2014**, *5*, 1–9.

(29) Broadwater Jr, D. B.; Kim, H. D. The effect of basepair mismatch on DNA strand displacement. *Biophysical journal* **2016**, *110*, 1476–1484.

(30) Šulc, P.; Romano, F.; Ouldridge, T. E.; Doye, J. P.; Louis, A. A. A nucleotide-level coarse-grained model of RNA. *The Journal of chemical physics* **2014**, *140*, 06B614_1.

(31) Šulc, P.; Ouldridge, T. E.; Romano, F.; Doye, J. P.; Louis, A. A. Modelling toehold-mediated RNA strand displacement. *Biophysical journal* **2015**, *108*, 1238–1247.

(32) Broadwater Jr, D. B.; Cook, A. W.; Kim, H. D. First passage time study of DNA strand displacement. *Biophysical Journal* **2021**,

(33) SantaLucia, J. A unified view of polymer, dumbbell, and oligonucleotide DNA nearest-neighbor thermodynamics. *Proceedings of the National Academy of Sciences* **1998**, *95*, 1460–1465.

(34) Sugimoto, N.; Nakano, S.-i.; Katoh, M.; Matsumura, A.; Nakamuta, H.; Ohmichi, T.; Yoneyama, M.; Sasaki, M. Thermodynamic parameters to predict stability of RNA/DNA hybrid duplexes. *Biochemistry* **1995**, *34*, 11211–11216.

(35) Serra, M. J.; Turner, D. H. *Methods in enzymology*; Elsevier, 1995; Vol. 259; pp 242–261.

(36) Ouldridge, T. E.; Šulc, P.; Romano, F.; Doye, J. P.; Louis, A. A. DNA hybridization kinetics: zippering, internal displacement and sequence dependence. *Nucleic acids research* **2013**, *41*, 8886–8895.

(37) Schaeffer, J. M.; Thachuk, C.; Winfree, E. Stochastic simulation of the kinetics of multiple interacting nucleic acid strands. International Workshop on DNA-Based Computers. 2015; pp 194–211.

(38) Zadeh, J. N.; Steenberg, C. D.; Bois, J. S.; Wolfe, B. R.; Pierce, M. B.; Khan, A. R.; Dirks, R. M.; Pierce, N. A. NUPACK: Analysis and design of nucleic acid systems. *Journal of computational chemistry* **2011**, *32*, 170–173.

Table of Contents Entry